Chapter 15

Sodium (^{23}Na) MRI of the Kidney: Basic Concept

James T. Grist, Esben Søvsø Hansen, Frank G. Zöllner, and Christoffer Laustsen

Abstract

The handling of sodium by the renal system is a key indicator of renal function. Alterations in the corticomedullary distribution of sodium are considered important indicators of pathology in renal diseases. The derangement of sodium handling can be noninvasively imaged using sodium magnetic resonance imaging (^{23}Na MRI), with data analysis allowing for the assessment of the corticomedullary sodium gradient. Here we introduce sodium imaging, describe the existing methods, and give an overview of preclinical sodium imaging applications to illustrate the utility and applicability of this technique for measuring renal sodium handling.

This chapter is based upon work from the COST Action PARENCHIMA, a community-driven network funded by the European Cooperation in Science and Technology (COST) program of the European Union, which aims to improve the reproducibility and standardization of renal MRI biomarkers. This introduction chapter is complemented by two separate chapters describing the experimental procedure and data analysis.

Key words Magnetic resonance imaging (MRI), Kidney, Mice, Rats, ^{23}Na, Sodium

1 Introduction

In this chapter, we describe renal sodium imaging, as acquired with magnetic resonance imaging (MRI). An introduction to the many methods that can be used to acquire sodium (23Na) signal is presented, as well as the postprocessing required to quantitatively describe the signal in terms of relaxation or concentration. Example applications of sodium renal imaging are discussed—ranging from the action of diuretic drugs to early sodium handling alterations in acute kidney injury. This introduction is complemented by two separate chapters describing the experimental procedure and data analysis, which are part of this book.

This chapter is part of the book Pohlmann A, Niendorf T (eds) (2020) Preclinical MRI of the Kidney—Methods and Protocols. Springer, New York.

Andreas Pohlmann and Thoralf Niendorf (eds.), *Preclinical MRI of the Kidney: Methods and Protocols*, Methods in Molecular Biology, vol. 2216, https://doi.org/10.1007/978-1-0716-0978-1_15,

2 Measurement Concept

2.1 Basic Concept of Sodium Imaging

Sodium imaging can provide quantitative measures of the ^{23}Na concentration in tissue [1]. It utilizes the signal from the sodium nucleus, found in both the intra- and extracellular compartments, to acquire images of the ^{23}Na biodistribution. Due to the low natural abundance of biological sodium, in comparison to water, as well as a rapid quadrupolar relaxation and lower gyromagnetic ratio (spin $= \frac{3}{2}$, $\gamma = 11.262 \frac{\text{MHz}}{\text{T}}$), approximately ¼ of protons, the signal available is much lower than that of conventional ^{1}H MRI [2]. The fast quadrupolar relaxation recovers some of the disadvantages of imaging ^{23}Na, as very short repetition times (TR) can be used, albeit the ultrafast T_2^* relaxation imposing constraints on the imaging technique used. Commonly, the total (meaning from both the intra- and extracellular compartments) sodium signal is acquired through the use of surface or RF volume coils, at high magnetic field strengths (3–9.4 T) using gradient echo-based imaging technique [3–6]. It is possible to suppress some of the extracellular signal, to give an "intracellular weighted" image, with advanced techniques such as inversion signal nulling or triple quantum filtering (TQF) [7, 8]. An estimate of the difference in the intra- and extracellular compartment sizes is feasible through the use of T_2^* mapping [9]. It is noted that no current use of TQF or inversion recovery signal nulling have been undertaken in renal studies; however, there are a number of publications in neurological work [8, 10, 11].

2.2 Sodium Imaging Methods

There are a number of imaging methods available for mapping the biodistribution of sodium in the renal system. The sodium signal detected in a simple imaging experiment is a combination of intra- and extracellular compartments, termed the "total" sodium signal. The three main methods used to differentiate the intra- and extracellular sodium signals are triple quantum filtering, inversion recovery fluid attenuation (IR), and T_2^* mapping.

2.2.1 Sodium MRI Hardware

For signal reception, the MR scanners need to be equipped by RF transmitters and receive RF coils tuned to the resonance frequency of the sodium nuclei at the respective magnetic field strength. Today, such extensions are supported by some vendors of preclinical systems. In the following, hardware developments for quantitative ^{23}Na-MRI in preclinical are briefly outlined.

For the first time, Barberi et al. introduced the transmit-only receive-only (TORO) system, the so-called dual radiofrequency (RF) resonator, which is based on the idea of separated transmit and receive RF elements [12]. In contrast to the standard RF resonators in transceiver (TXRX) mode (e.g., surface coil or

birdcage), the dual RF resonator allows for both a homogeneous transmit B_1^+ field and a highly sensitive receive B_1^- field [12, 13].

Kalacycian et al. developed a homogeneous transmit-only volume resonator and a highly sensitive RO surface resonator for renal ^{23}Na-MRI for 3 T or 9.4 T MRI scanners [14]. For this setup the sensitivity correction needs to be performed only for the receive profile. Furthermore, the dual resonator allows for increased ^{23}Na-MR signal sensitivity due to the localized signal detection using RO surface coils. For the dedicated task of bilateral kidney imaging, a dual resonator system (TORO) including a two-element phased array at 9.4 T and a receiver saddle shaped RF resonator at 3 T was implemented [13]. These systems were tailored for measuring the absolute renal TSC in rat kidney models with high spatiotemporal resolution, and high concentration measurement accuracy.

2.2.2 Total Sodium Imaging

Total sodium imaging is typically performed using a gradient echo-based technique. To ensure that the conversion from the imaging signal to the sodium concentration is accurate, a repetition time of approximately 2.5 times the T_1 of tissue sodium (approximately 25 ms at 3 T, and longer at higher field strengths) is essential. Further optimization of the sequence readout can be undertaken to capture the fast T_2^* relaxation of the sodium nucleus. For example, an ultrashort echo time (UTE) approach such as radial or twisted projection imaging is preferred over conventional Cartesian strategies. Due to the inherent low SNR of sodium acquisitions, it is common to average a number of sodium scans from the same subject; however, this may lead to long scan times.

An example of total sodium imaging pulse sequence, and renal images, are provided in Figs. 1a and 2.

2.2.3 Triple Quantum Filtering (TQF)

Due to the $\frac{3}{2}$ spin of the sodium nucleus, a biexponential T_2^* is exhibited by the isotope. A single excitation with a 90-degree hard pulse causes a transition of spins between the outer spin states ($\frac{3}{2}$ to $\frac{1}{2}$ and $-\frac{1}{2}$ to $-\frac{3}{2}$) as well as the inner states ($\frac{1}{2}$ to $-\frac{1}{2}$). The outer spin states exhibit a faster T_2^* decay than the inner. Using phase-cycled radiofrequency pulses it is possible to isolate the signal of slow-moving spins in the intracellular compartment, while removing the extracellular contribution [15].

There are a number of limitations to TQF though. The challenges include long scan times and high energy deposition required due to a large SNR penalty of the TQF technique. Furthermore, inhomogeneity in main magnetic field distribution can lead to spurious results, with corrections in reconstruction required to counter the B_0-nonuniformity effects [10]. An example triple quantum filtering sodium imaging pulse sequence is shown in Fig. 1b.

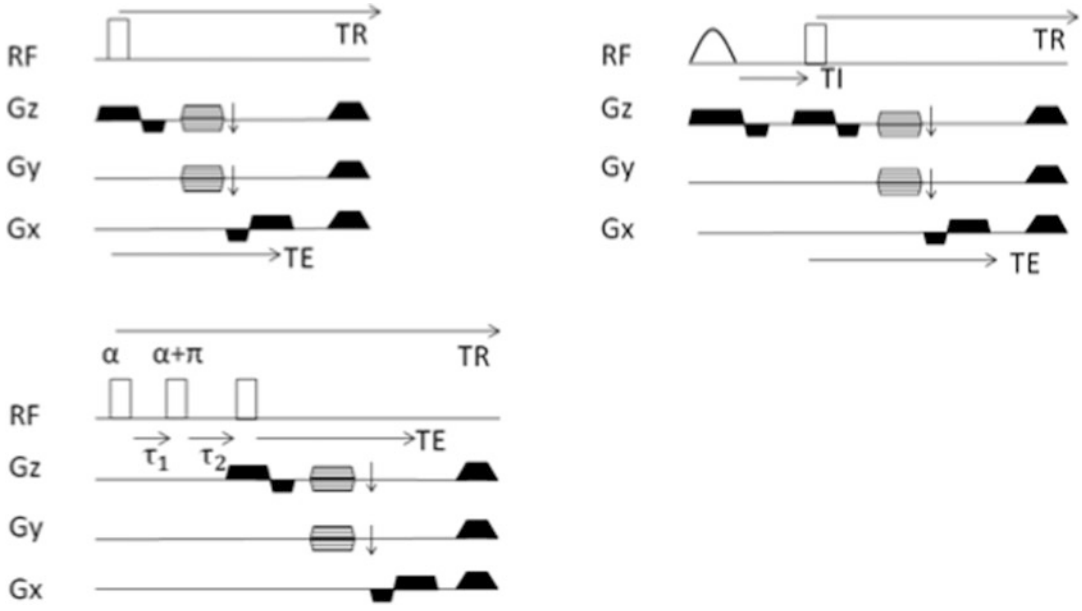

Fig. 1 Sodium imaging pulse sequences. (**a**) Total sodium imaging sequence using a 3D GRE readout. TR = Repetition time, TE = Echo time. (**b**) Triple Quantum Filtered sodium imaging pulse sequence using a 3D GRE readout. α = phase of pulse 1, T1 = Mixing time 1, T2 = Mixing time 2. (**c**) Inversion prepared sodium imaging pulse sequence. TI = Inversion preparation time (determined experimentally)

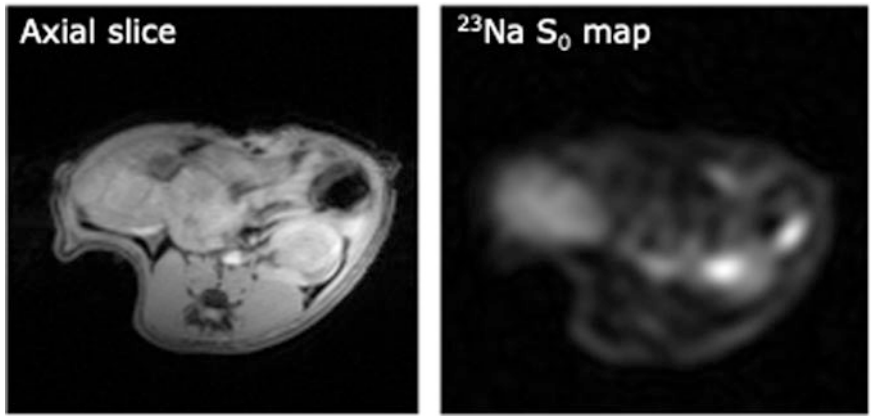

Fig. 2 Example rodent renal ^{1}H (left) and sodium (right) imaging acquired at 9.4 T

2.2.4 Inversion Recovery Utilizing the difference in T_1 between bound and unbound sodium, it is possible to null the signal contribution fluid compartment using an inversion pulse, whilst retaining the bound signal, as described through Eqs. 1 and 2 [7].

$$S(\mathrm{TI}) = S_0\left(1 - \exp\left(-\frac{\mathrm{TI}}{T_1}\right)\right) \tag{1}$$

$$\mathrm{TI}_{\mathrm{null}} = \ln(2)\, T_1^{\mathrm{Fluid}} \tag{2}$$

where TI is the inversion time, T_1 is the relaxation constant of free sodium, S_0 is the initial sodium NMR signal, and S(TI) is the signal at TI. An example of an inversion recovery sodium imaging technique is illustrated in Fig. 1c.

2.2.5 T2* Mapping

T_2^* mapping is performed with either a multiecho based gradient echo sequence, or many individual scans with an incremented echo time (TE). It is currently thought that the shorter T_2^* component (1-5 ms at 3 T) is derived from the intracellular compartment, and the longer (10–30 ms at 3 T) from the extracellular compartment [9, 16]. T2* mapping therefore could be sensitive to changes in the intracellular–extracellular renal sodium balance.

A multiecho or incremented echo series can be used to derive both the pool sizes and T_2^* time constant for each compartment through Eq. 3.

$$S(\mathrm{TE}) = \left(a \exp\left(-\frac{\mathrm{TE}}{T^*_{2,\mathrm{Short}}} \right) + b \exp\left(-\frac{\mathrm{TE}}{T^*_{2,\mathrm{Long}}} \right) \right) \quad (3)$$

where S(TE) is the signal at a given echo time, a and b are the intra- and extracellular pool sizes, respectively, and $T^*_{2,\mathrm{Short}}$ and $T^*_{2,\mathrm{Long}}$ are the biexponential relaxation constants.

2.3 Imaging Readout

Due to the rapid decay of the sodium signal, fast gradient echo-based imaging methods are commonly employed for data acquisition. A large number of encoding schemes are present in the literature, encompassing Cartesian and non-Cartesian imaging [17]. Below is a summary of most frequently applied methods.

2.3.1 3D Cartesian Imaging

The majority of preclinical imaging has been undertaken with 3D gradient echo Cartesian imaging, whereby a volume of k-space is sampled using trapezoidal readout gradients. Due to the ease of implementation on a preclinical system, this has been the sequence of choice for a number studies in rodents [3–5]. However, as Cartesian imaging requires encoding in k_y and k_z directions prior to data acquisition, the minimum echo time available for imaging is substantially longer than in other methods available for use in future studies.

2.3.2 Ultrashort Echo Time (UTE) Imaging

In order to shorten the echo time of acquisition, thereby increasing the total signal available for sampling, non-Cartesian imaging trajectories can be employed. Non-Cartesian trajectories are less commonly used in imaging, and require special design of magnetic field gradient waveforms and a more sophisticated reconstruction process. However, with a very short minimum echo time, 3D non-Cartesian trajectories are better suited for probing the fast-relaxing sodium signal. Where a 3D Cartesian sequence requires localisation in k_y and k_z prior to data acquisition, a 3D non-Cartesian acquisition starts each excitation at the center of k-space, and data are simultaneously acquired in k_x, k_y, and k_z. To

ensure short TE in UTE imaging a hard RF pulse is commonly used to excite all spins in the imaging volume. A number of trajectories used for non-Cartesian data readout are available from literature, for example radial imaging, twisted projection imaging (TPI), density adapted radial (DAR) imaging, and 3D CONES, briefly described in the following.

Twisted projection imaging (TPI) was first described by Fernando Boada in 1997, as an extension to 2D TWIRL imaging [18]. The technique utilizes a hybrid radial-spiral sampling of k-space, allowing for acceleration in comparison to radial imaging with an underdamping factor defined during trajectory construction. TPI requires high gradient slew rates for image acquisition, due to the sharp transition between the radial and spiral potions of the trajectory. Further optimizations to the trajectory can be made by optimizing maximum gradient amplitudes throughout scan time [19].

Density adapted radial (DAR) trajectories are described in work by Nagel, whereby concentric rings of k-space are acquired with a radial readout. DAR allows for under sampling of k-space, shortening acquisition times in comparison to radial imaging [20].

The 3D cones approach was initially described for UTE proton imaging and has found applications in sodium acquisitions [21, 22]. Due to the high *k*-space efficiency of the trajectory, it is possible to acquire a full imaging volume in a very short time, leading to rapid high resolution imaging [23]. However, due to the high k-space efficiency, the SNR of each volume is lower than a radial acquisition; therefore, it is common practice to perform a number of spatial averages in a single acquisition.

2.4 Reconstruction

There are three main methods for reconstruction of sodium imaging data, depending on the acquisition scheme used. If Cartesian data is acquired, a Fourier transform is applied in all dimensions (x, y,z,t). If non-Cartesian acquisitions are employed more complex reconstruction strategies such as gridding or nonuniform fast Fourier transforms are used. Compensation for the oversampling of the center of k-space is performed in non-Cartesian imaging using precalculated density compensation functions (*see* **Note 1**).

2.5 Sodium Phantoms

External calibration phantoms are used to convert sodium imaging data to quantitative maps, with voxels fitted to a calibration curve formed from measurements of signal from known concentration phantoms as well as from regions of noise in the image.

Phantoms are generally made from agarose doped with sodium chloride, to ensure a T_1 and T_2 that mimic that of tissue. However, other designs are also possible. Phantoms are placed within the imaging field of view before the start of the experiment to ensure that signal is acquired from both tissue and calibration standards in the same exam.

2.6 Segmentation

Segmentation of the kidney is commonly achieved through region of interests initially drawn on proton anatomical imaging and transferred to the sodium images. Other methods have been proposed for the segmentation of the renal system, in particular to measure the corticomedullary sodium gradient, focusing on defining layers of the kidney from an initial whole kidney region [24].

3 Overview of Applications

3.1 Total sodium Imaging for Assessing Alterations in the Corticomedullary sodium Gradient

The corticomedullary sodium gradient has been studied with sodium imaging in a number of healthy and pathological scenarios [3–5, 25–29]. Broadly, the current preclinical literature focuses either on the action of diuretic drugs upon the sodium gradient, or upon acute tubular necrosis. The action of furosemide has been estimated by acquiring longitudinal imaging before and after the introduction of the acute diuretic. Furosemide acts as a loop diuretic, halting reabsorption of sodium through the loop of Henley, leading to acute diuresis. Results from studies have shown the capability of sodium MRI to detect the acute renal sodium alterations induced by furosemide, revealing a flattening of the corticomedullary sodium gradient within minutes of administration [3, 4, 26].

Studies focusing upon the early formation of acute kidney injury through tubular necrosis have revealed alterations in the sodium gradient, with a decreased gradient in the damaged kidney [5].

3.2 Potential Future Applications of sodium Imaging

Although the literature is limited to the current applications of renal sodium imaging, there is a large scope for further preclinical studies demonstrating the power of this technique to probe disease formation. In particular, the formation of acute kidney disease and chronic kidney disease remain prime targets for further ^{23}Na MRI studies.

3.3 Acute Kidney Disease

Acute kidney disease is heralded by a sudden loss of renal function, and impaired reabsorption of electrolytes such as urea and sodium [30]. Indeed, this is a key clinical problem, with a number of patients diagnosed upon admission with AKI and leads to high mortality rates. AKI can occur over a number of hours or days, and is heralded by an decrease of the glomerular filtration rate, leading to retention of nitrogenous waste [31]. Due to the increase in waste retention, common methods for diagnosis are serum-based measures of creatinine clearance and blood nitrogen [31]. Further to the increase in the retention of waste, sodium reabsorption is impaired in AKI. An initial sodium imaging study showed a flattening of the corticomedullary sodium gradient [32]. A particular challenge in diagnosis and management of AKI is the direct estimation of renal health and function pre- and post-therapy, with many imaging methods either requiring the

introduction of potentially hazardous contrast agents, or unable to provide physiological information [33]. Here sodium imaging may provide a more specific measure of renal health. The initial imaging study, mentioned above, offers a potential for further studies assessing therapeutic response [32]. Assessing the angle of the corticomedullary sodium gradient may also provide insights in to the degree of the insult that the disrupted kidney is facing.

3.4 Chronic Kidney Disease

Chronic kidney disease (CKD) is characterized by a gradual loss of kidney function over time, leading to a decrease in the intrarenal transport of metabolites such as urea and sodium [34, 35]. A challenge in this disease is, as with AKI, both monitoring disease progression and estimating therapeutic response. Sodium imaging has the potential to evaluate renal function via the corticomedullary sodium gradient, to differentiate the earliest changes in the metabolic and functional mismatch that occur in the renal system prior to the development of kidney disease [28, 32, 36]. The use of a combined multimodal anatomical and functional imaging approach with methods such as sodium, arterial spin labeling, BOLD, dynamic contrast enhanced imaging, and diffusion weighted imaging may provide a more complete picture of the alterations in renal function in relation to chronic kidney disease [24, 36–42].

4 Notes

1. Example gridding and density compensation calculation functions used for the reconstruction of data acquired with non-Cartesian trajectories can be found at https://www.ismrm.org/mri_unbound/sequence.htm.

Acknowledgments

The authors would like to thank Andreas Pohlmann and Thoralf Niendorf for assistance in preparing this chapter (Max-Delbrück Center for Molecular Medicine in the Helmholtz Association, Berlin, Germany.
This chapter is based upon work from COST Action PARENCHIMA, supported by European Cooperation in Science and Technology (COST). COST (www.cost.eu) is a funding agency for research and innovation networks. COST Actions help connect research initiatives across Europe and enable scientists to enrich their ideas by sharing them with their peers. This boosts their research, career, and innovation.
PARENCHIMA (renalmri.org) is a community-driven Action in the COST program of the European Union, which unites more than 200 experts in renal MRI from 30 countries with the aim to improve the reproducibility and standardization of renal MRI biomarkers.

References

1. Christensen JD, Barrère BJ, Boada FE et al (1996) Quantitative tissue sodium concentration mapping of normal rat brain. Magn Reson Med 36:83–89
2. Zöllner FG, Konstandin S, Lommen J et al (2016) Quantitative sodium MRI of kidney. NMR Biomed 29:197–205
3. Maril N, Margalit R, Mispelter J, Degani H (2004) Functional sodium magnetic resonance imaging of the intact rat kidney. Kidney Int 65:927–935
4. Maril N, Margalit R, Mispelter J, Degani H (2005) Sodium magnetic resonance imaging of diuresis: spatial and kinetic response. Magn Reson Med 53:545–552
5. Maril N, Margalit R, Rosen S et al (2006) Detection of evolving acute tubular necrosis with renal 23Na MRI: studies in rats. Kidney Int 69:765–768
6. Zöllner FG, Kalayciyan R, Chacón-Caldera J et al (2014) Pre-clinical functional magnetic resonance imaging part I: the kidney. Z Med Phys 24:286–306
7. Stobbe R, Beaulieu C (2005) In vivo sodium magnetic resonance imaging of the human brain using soft inversion recovery fluid attenuation. Magn Reson Med 54:1305–1310
8. Benkhedah N, Bachert P, Semmler W, Nagel AM (2012) Three-dimensional biexponential weighted (23) Na imaging of the human brain with higher SNR and shorter acquisition time. Magn Reson Med 765:754–765
9. Riemer F, Solanky BS, Wheeler-Kingshott CAM, Golay X (2018) Bi-exponential ^{23} Na T_2 * component analysis in the human brain. NMR Biomed 31(5):e3899
10. Tsang A, Stobbe RW, Beaulieu C (2013) Evaluation of B0-inhomogeneity correction for triple-quantum-filtered sodium MRI of the human brain at 4.7 T. J Magn Reson 230:134–144
11. Hancu I, Boada FE, Shen GX (1999) Three-dimensional triple-quantum-filtered 23Na imaging of in vivo human brain. Magn Reson Med 42:1146–1154
12. Ackerman JJH, Grove TH, Wong GG et al (1980) Mapping of metabolites in whole animals by 31P NMR using surface coils. Nature 283:2–5
13. Mueller OM, Hayes CE, Eash M et al (2006) An efficient, highly homogeneous radiofrequency coil for whole-body NMR imaging at 1.5 T. J Magn Reson 63:622–628
14. Kalayciyan R, Malzacher M, Neudecker S, Gretz N SL (2013) 23Na/1H in-vivo renal MRI of rodent kidney at 3T by using a double-tuned transceiver resonator system. In: International Society for Magnetic Resonance in Medicine. Salt-Lake City, p 4355
15. Hancu I, Boada FE, Shen GX (1999) Three-dimensional triple-quantum – filtered 23 Na imaging of in vivo human brain. Magn Reson Med 42(6):1146–1154
16. Qian Y, Panigrahy A, Laymon CM et al (2014) Short-T2 imaging for quantifying concentration of sodium ((23) Na) of bi-exponential T2 relaxation. Magn Reson Med 00:00–00
17. Konstandin S, Nagel AM (2014) Measurement techniques for magnetic resonance imaging of fast relaxing nuclei. MAGMA 27:5–19
18. Boada FE, Gillen JS, Shen GX et al (1997) Fast three dimensional sodium imaging. Magn Reson Med 37:706–715
19. Angelica MD, Fong Y (2008) Quantitative sodium imaging with a flexible twisted projection pulse sequence. Magn Reson Med 141:520–529
20. Nagel AM, Laun FB, Weber M-A et al (2009) Sodium MRI using a density-adapted 3D radial acquisition technique. Magn Reson Med 62:1565–1573
21. Riemer F, Solanky BS, Stehning C et al (2014) Sodium (23Na) ultra-short echo time imaging in the human brain using a 3D-Cones trajectory. MAGMA 27:35–46
22. Gurney PT, Hargreaves BA, Nishimura DG (2006) Design and analysis of a practical 3D cones trajectory. Magn Reson Med 55:575–582
23. Grist JT, Riemer F, McLean MA et al (2018) Imaging intralesional heterogeneity of sodium concentration in multiple sclerosis: initial evidence from 23Na-MRI. J Neurol Sci 387:111–114
24. Milani B, Ansaloni A, Sousa-Guimaraes S et al (2016) Reduction of cortical oxygenation in chronic kidney disease: evidence obtained with a new analysis method of blood oxygenation level-dependent magnetic resonance imaging. Nephrol Dial Transplant 32 (12):2097–2105
25. Maril N, Rosen Y, Reynolds GH et al (2006) Sodium MRI of the human kidney at 3 tesla. Magn Reson Med 56:1229–1234
26. Neuberger T, Gulani V, Webb A (2007) Sodium renal imaging in mice at high magnetic fields. Magn Reson Med 58:1067–1071
27. Haneder S, Juras V, Michaely HJ et al (2014) In vivo sodium (23Na) imaging of the human

kidneys at 7 T: preliminary results. Eur Radiol 24:494–501
28. Qi H, Nørlinger TS, Nielsen PM et al (2016) Early diabetic kidney maintains the corticomedullary urea and sodium gradient. Physiol Rep 4:1–6
29. Giovannetti G, Pingitore A, Positano V et al (2014) Improving sodium magnetic resonance in humans by design of a dedicated 23Na surface coil. Measurement 50:285–292
30. Hansell P, Welch WJ, Blantz RC, Palm F (2013) Determinants of kidney oxygen consumption and their relationship to tissue oxygen tension in diabetes and hypertension. Clin Exp Pharmacol Physiol 40:123–137
31. Basile DP, Anderson MD, Sutton TA (2012) Pathophysiology of acute kidney injury. Compr Physiol 2:1303–1353
32. Nielsen PM, Szocska Hansen ES, Nørlinger TS et al (2016) Renal ischemia and reperfusion assessment with three-dimensional hyperpolarized13C,15N2-urea. Magn Reson Med 76:1524–1530
33. Perazella MA (2015) Gadolinium-contrast toxicity in patients with kidney disease: nephrotoxicity and nephrogenic systemic fibrosis. Curr Drug Saf 3:67–75
34. McFarland JG (1999) Perioperative blood transfusions: indications and options. Chest 115:113S–121S
35. Thomas R, Kanso A, Sedor JR (2008) Chronic kidney disease and its complications. Prim Care 35:329–344
36. Bertelsen LB, Nielsen PM, Qi H et al (2017) Diabetes induced renal urea transport alterations assessed with 3D hyperpolarized13C,15N-urea. Magn Reson Med 77:1650–1655
37. Cox EF, Buchanan CE, Bradley CR et al (2017) Multiparametric renal magnetic resonance imaging: validation, interventions, and alterations in chronic kidney disease. Front Physiol 8:1–15
38. Piskunowicz M, Hofmann L, Zuercher E et al (2015) A new technique with high reproducibility to estimate renal oxygenation using BOLD-MRI in chronic kidney disease. Magn Reson Imaging 33:253–261
39. Pruijm M, Milani B, Burnier M (2017) Blood oxygenation level-dependent mri to assess renal oxygenation in renal diseases: progresses and challenges. Front Physiol 7:1–7
40. Nielsen PM, Eldirdiri A, Bertelsen LB et al (2017) Fumarase activity: an in vivo and in vitro biomarker for acute kidney injury. Sci Rep 7:40812
41. Zimmer F, Zöllner FG, Hoeger S et al (2013) Quantitative renal perfusion measurements in a rat model of acute kidney injury at 3T: testing inter- and intramethodical significance of ASL and DCE-MRI. PLoS One 8:e53849
42. Zhou HY, Chen TW, Zhang XM (2016) Functional magnetic resonance imaging in acute kidney injury: present status. Biomed Res Int 2016:2027370